

Enhanced spin-orbit torque efficiency in Pt/Co/Ho heterostructures via inserting Ho layer

Cite as: APL Mater. 8, 111111 (2020); <https://doi.org/10.1063/5.0029451>

Submitted: 15 September 2020 . Accepted: 04 November 2020 . Published Online: 20 November 2020

 Tianli Jin,  Wai Cheung Law, Durgesh Kumar, Feilong Luo,  Qi Ying Wong,  Gerard Joseph Lim, Xuan Wang,  Wen Siang Lew, and  S. N. Piramanayagam



View Online



Export Citation



CrossMark

additive manufacturing epitaxial crystal growth cerium oxide polishing powder silver nanoparticles sputtering targets



AMERICAN ELEMENTS

THE ADVANCED MATERIALS MANUFACTURER®

deposition slugs OLED Lighting spintronics solar energy

osmium nanoribbons thin films chalcogenides AuNPs

GDC li-ion battery electrolytes 99.999% ruthenium spheres

endohedral fullerenes copper nanoparticles diamond micropowder

CIGS MBE grade materials palladium catalysts flexible electronics

beta-barium borate borosilicate glass dysprosium pellets YBCO

pyrolytic graphite 3d graphene foam indium tin oxide mesoporous silica

raman substrates sapphire windows tungsten carbide InGaAs

barium fluoride carbon nanotubes lithium niobate scandium powder



gallium lump glassy carbon nanodispersions

surface functionalized nanoparticles organometallics quantum dot

III-IV semiconductors CVD precursors europium phosphors

InAs wafers laser crystals ultra high purity materials MOFs

rare earth metals photovoltaics refractory metals MOCVD

superconductors transparent ceramics ultra high purity silicon

*American Elements opens up a world of possibilities so you can **Now Invent!***

Over 15,000 certified high purity laboratory chemicals, metals, & advanced materials and a state-of-the-art Research Center. Printable GHS-compliant Safety Data Sheets. Thousands of new products. And much more. All on a secure multi-language "Mobile Responsive" platform.

perovskite crystals yttrium iron garnet alternative energy h-BN

gold nanocubes graphene oxide macromolecules photonics

rhodium sponge fiber optics beamsplitters infrared dyes zeolites

fused quartz metallocenes platinum ink buckyballs Ti-6Al-4V

Now Invent.™
The Next Generation of Material Science Catalogs

www.americanelements.com



Enhanced spin-orbit torque efficiency in Pt/Co/Ho heterostructures via inserting Ho layer

Cite as: *APL Mater.* **8**, 111111 (2020); doi: [10.1063/5.0029451](https://doi.org/10.1063/5.0029451)
Submitted: 15 September 2020 • Accepted: 4 November 2020 •
Published Online: 20 November 2020



Tianli Jin,¹ Wai Cheung Law,¹ Durgesh Kumar,¹ Feilong Luo,¹ Qi Ying Wong,¹ Gerard Joseph Lim,¹
Xuan Wang,² Wen Siang Lew,^{1,a)} and S. N. Piramanayagam^{1,a)}

AFFILIATIONS

¹School of Physical and Mathematical Sciences, Nanyang Technological University, Singapore 637371, Singapore

²School of Science, Lanzhou University of Technology, Lanzhou 730050, China

^{a)}Authors to whom correspondence should be addressed: wensiang@ntu.edu.sg and prem@ntu.edu.sg

ABSTRACT

Spin-orbit torque (SOT) is a promising approach to manipulate the magnetization for high-performance spintronic applications. In conventional SOT heterostructures with heavy metal (HM)/ferromagnet layers, the SOT efficiency is determined by the charge-to-spin conversion, characterized by the spin Hall angle θ_{SH} of the HM layer. Researchers have investigated various HMs with different θ_{SH} to enhance the SOT efficiency while it is still limited because of the HM's intrinsic properties. In this study, we employ a rare-earth holmium (Ho) layer on top of a ferromagnetic Co layer (Pt/Co/Ho) to enhance the SOT efficiency. An increased damping-like SOT efficiency up to 200% is achieved at an optimized thickness of 2-nm Ho, corresponding to a lower switching current density, which is 60% less compared to the sample without a Ho layer. The damping-like torque efficiency per current density is estimated at around 0.256 for Pt/Co/Ho heterostructures. Our results, herein, demonstrate that inserting a rare-earth metal affords an additional spin current and/or improves the spin transparency to enhance the SOT efficiency, providing a route for energy-efficient spintronic devices.

© 2020 Author(s). All article content, except where otherwise noted, is licensed under a Creative Commons Attribution (CC BY) license (<http://creativecommons.org/licenses/by/4.0/>). <https://doi.org/10.1063/5.0029451>

Researchers aim at developing spin-based logic and memory devices with high-energy efficiency and fast operational speed.^{1–5} Conventionally, the magnetic random-access memory (MRAM) devices, utilizing spin-transfer torque (STT) mechanism to write information, have been introduced in consumer electronics. The STT-MRAM can exhibit up to 1000 times faster than the current NAND flash.⁶ However, the STT-MRAM suffers from reliability concerns and high endurance issues arising from the high-density current that flows through the tunnel barrier during the write operation.⁷ The erroneous writing that may occur during a read operation by the readout current is another drawback.^{8,9} In order to overcome those drawbacks of STT-MRAM, an alternative MRAM technology based on spin-orbit torque (SOT), viz., SOT-MRAM, has been proposed. An SOT-MRAM uses separate paths for sending writing and reading currents. Therefore, the SOT-MRAM shows better performance with faster access time, lower energy consumption, better endurance, and fewer disturbance errors.^{10,11}

In the SOT-MRAM, a charge current that flows through the heavy metal (HM) layer generates spin current due to the bulk spin Hall effect (SHE)^{1,4,12,13} and/or the interfacial Rashba–Edelstein effect.¹⁴ The spin current exerts a torque on the adjacent magnetic layer, thus causing the magnetization reversal. Here, the spin-torques are generally treated as two orthogonal components, damping-like (DL) torque and field-like (FL) torque. The ratio of the spin current to charge current is known as the spin Hall angle θ_{SH} . Studies have revealed that the magnetization switching is mainly driven by the DL torque, which is proportional to θ_{SH} .^{15–17} Therefore, materials with large θ_{SH} are significantly desired for achieving high SOT efficiency.^{1,18,19} Recently, SOT-induced switching has been demonstrated in magnetic multilayers in contact with larger θ_{SH} materials, such as heavy metals (Ta and W)^{18,20–22} and topological insulators (Bi₂Se₃).^{23,24} For example, β -W exhibits a large spin Hall angle ($\theta_{SH} \sim -0.30$ to -0.62),^{18,25,26} as compared to Pt ($\theta_{SH} \sim 0.09$).^{1,21} A large θ_{SH} is still being pursued for a higher SOT efficiency.

Furthermore, engineering on materials such as alloying HM^{17,27} and inserting antiferromagnetic layers²⁸ to enhance the spin generation and spin transparency have been demonstrated to further improve the SOT efficiency. In addition to the aforementioned heavy metals, alternative approaches by inserting rare-earth metals have been proposed to enhance the SOT efficiency. Some studies have verified the positive function of rare-earth metals, like Tb^{29,30} and Gd,³¹ in improving the SOT efficiency due to its large spin-orbit coupling, as well as the negative exchange interaction between the ferromagnetic layer and rare-earth Tb/Gd sublattices.^{31–33}

In this work, we report the significant SOT enhancement in Pt/Co/Ho heterostructures via employing a rare-earth metal Ho layer. We observe that the critical switching current density is reduced by 60% compared to Pt/Co heterostructures without a Ho layer by performing the current-induced magnetization switching measurements. The enhancement in the SOT switching efficiency is consistent with the harmonic measurements. Moreover, we find that the damping-like SOT efficiency increasing by 200% is achieved

at an optimized Ho insertion thickness of 2 nm. Our results demonstrate an efficient approach to improve the SOT efficiency by inserting rare-earth metal Ho, which are important for technological applications.

The samples of Pt (5 nm)/Co (1.2 nm)/Ho (t_{Ho})/MgO (5 nm)/Ta (2 nm) structures were investigated in this work. The thin film stacks were deposited by direct current (DC) sputtering and radio frequency (RF) sputtering onto thermally oxidized Si substrates in a vacuum system with a base pressure of 5×10^{-8} Torr. The thickness of the Ho layer t_{Ho} was varied from 1 nm to 10 nm. The control sample, Pt (5 nm)/Co (1.2 nm)/MgO (5 nm)/Ta (2 nm) without Ho, abbreviated as Pt/Co/MgO, was also prepared for comparison. The schematic illustration of the film stack is shown in Fig. 1(a). Subsequently, the Hall bar patterned devices were fabricated with the configurations of $5 \mu\text{m}$ -width and $50 \mu\text{m}$ -length using electron-beam lithography and Ar ion-beam etching techniques, as shown in Fig. 1(b). The magnetic properties of the deposited thin films were investigated by a vibrating sample magnetometer (VSM). The device

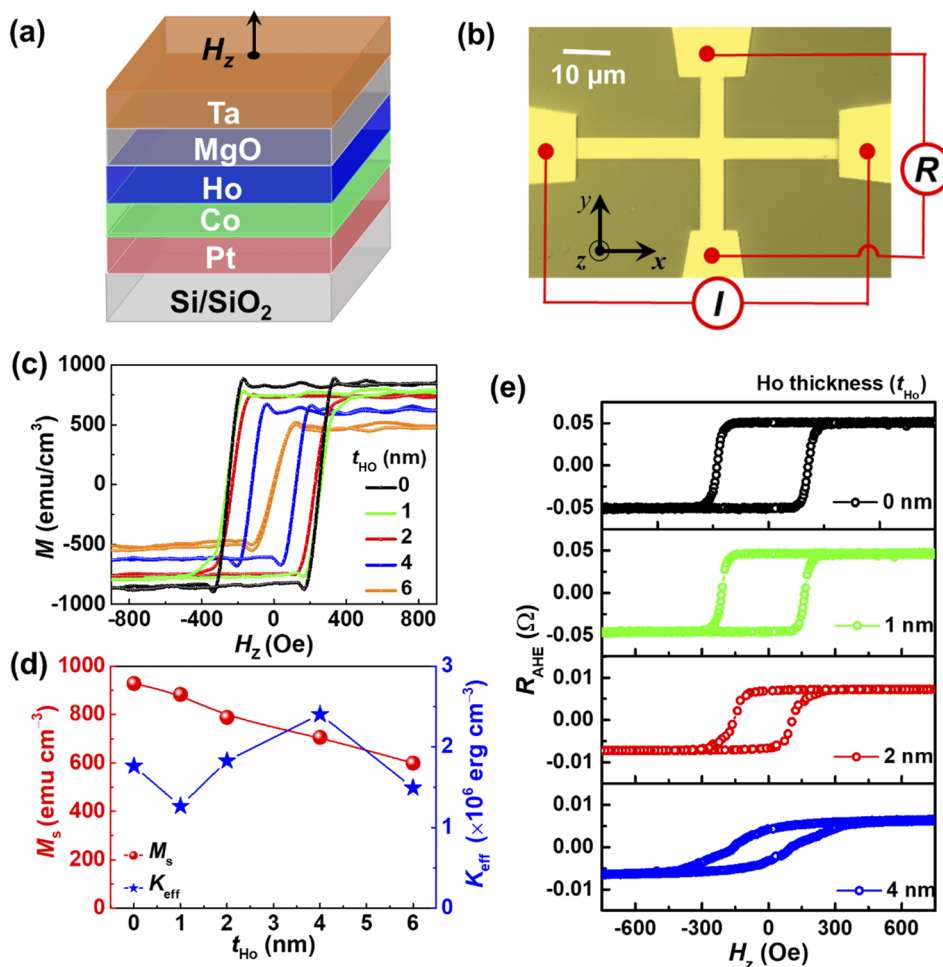


FIG. 1. (a) A schematic illustration of the sample structure Pt/Co/Ho(t_{Ho})/MgO/Ta multilayer. (b) Microscope image of the investigated Hall bar device and the Hall resistance experimental configuration. (c) The magnetic hysteresis loops of Pt/Co/Ho (t_{Ho}) samples measured by the vibrating sample magnetometer. (d) The saturation magnetization M_s and effective magnetic anisotropy constant K_{eff} for the investigated films with different insertion thicknesses of the Ho layer (t_{Ho}). (e) Anomalous Hall resistance as a function of out-of-plane magnetic field, $R_{\text{AHE}}-H_z$, for samples with Ho thickness from 0 nm to 4 nm.

properties were characterized by anomalous Hall effect (AHE) measurements. The effective magnetic field induced by SOTs was determined using a harmonic lock-in technique. All measurements were performed at room temperature.

We first investigated the modification on magnetic properties by inserting different thicknesses of the Ho layer. Figure 1(c) shows the out-of-plane (OOP) magnetic hysteresis ($M-H_z$) loops of the film stacks with the Ho thickness varying from 0 nm to 6 nm. The square hysteresis loops indicate a good perpendicular magnetic anisotropy (PMA) of the samples with normalized remanence M_r/M_s larger than 90%, arising from the Pt/Co interface.³⁴ The loops become narrower with the increase of Ho thickness, which indicates a reduction of coercivity field H_c . For t_{Ho} above 6 nm, the normalized remanence M_r/M_s gradually reduces to zero. The results with Ho thickness above 6 nm have been shown in Fig. S1 of the supplementary material. The saturation magnetization M_s shows a steady decrease from $928 \pm 10 \text{ emu cm}^{-3}$ ($t_{\text{Ho}} = 0 \text{ nm}$) to $600 \pm 12 \text{ emu cm}^{-3}$ ($t_{\text{Ho}} = 6 \text{ nm}$) with the increase of Ho thickness, as shown in Fig. 1(d). M_s was mainly determined by the total magnetic moment averaged over the volume of the Co layer. When the thickness of Ho increases to 10 nm, the larger reduction in M_s to $486 \pm 15 \text{ emu cm}^{-3}$ happens. The reduction in M_s is due to the larger diffusion of Ho into the Co layer at the Co/Ho interface for the thicker Ho samples,³⁵ which was further verified by the transport of ions in matter (TRIM) simulations (refer to Sec. S2 of the supplementary material).

To gain more understanding of the modification on magnetic properties, we have calculated the effective magnetic anisotropy K_{eff} , as shown in Fig. 1(d). K_{eff} was determined by the enclosed area within the hysteresis loops along OOP and in-plane (IP) directions.³⁴ K_{eff} shows an initial increase, followed by a decrease for a further increase of t_{Ho} . K_{eff} is mainly determined by the interface and strain anisotropy energies in the ultrathin layered system. In the sample without Ho, the Co magnetic moments align to the (111) direction due to the high interfacial anisotropy of the Pt/Co interface, resulting in a strong perpendicular anisotropy. For samples with a thin Ho layer, low concentrations of a rare-earth substituted

Co alloy may form due to the diffusion of Ho. In this case, atomic-scale structural anisotropy (pair-ordering) may occur, similar to the magnetic anisotropy observed in magneto-optical recording materials.³⁶ With further increasing Ho thickness, inter-diffusion from Ho to Co happens strongly to reduce both the interfacial anisotropy and the pair-ordering anisotropy. Therefore, K_{eff} decreases as the increase of the insertion thickness of Ho. These results indicate that the Pt/Co films exhibit suitable PMA and the introduction of a Co/Ho interface is not detrimental for t_{Ho} up to 4 nm. Magnetic materials with PMA are promising to achieve a higher storage density and thermal stability compared to materials with IP anisotropy. Therefore, subsequent studies are mainly focused on samples that exhibit PMA in this work. Figure 1(e) shows the anomalous Hall resistance $R_{\text{AHE}}-H_z$ loops of the samples in the Hall bar devices. For t_{Ho} less than 4 nm, R_{AHE} shows square loops, confirming the PMA property of the devices, in good agreement with the $M-H_z$ loops in Fig. 1(c). The sample with $t_{\text{Ho}} = 4 \text{ nm}$, which exhibits a squareness close to 1 in the $M-H_z$ loops, shows a lower value of squareness in $R_{\text{AHE}}-H_z$ measurements. The samples start to show the degradation of PMA after fabricating from thin films. Therefore, the following experiments and discussions are mainly focused on the samples with insertion Ho thickness no more than 4 nm, which show a PMA and indicate a thickness practical for most applications.

In order to evaluate the effect on the SOT efficiency by inserting different thicknesses of the Ho layer, current-induced magnetization switching was subsequently performed on these devices. Figure 2(a) shows a schematic of the spin orientation \hat{p} of the electrons diffusing into the Co layer when a current (J) was sent through the Pt/Co/Ho stack. The spin current at the Co layer generates DL and FL effective fields, which exert torques to switch the magnetization. The DL and FL fields can be expressed as $a_j \hat{m} \times \hat{p}$ and $b_j \hat{p}$, respectively, where \hat{m} represents the magnetization direction of the magnetic layer and a_j and b_j depend on the status of the magnetization, indicating the magnitudes of the corresponding fields.³⁷

Figure 2(b) shows the current-induced magnetization switching loops by varying the external IP magnetic field H_x from

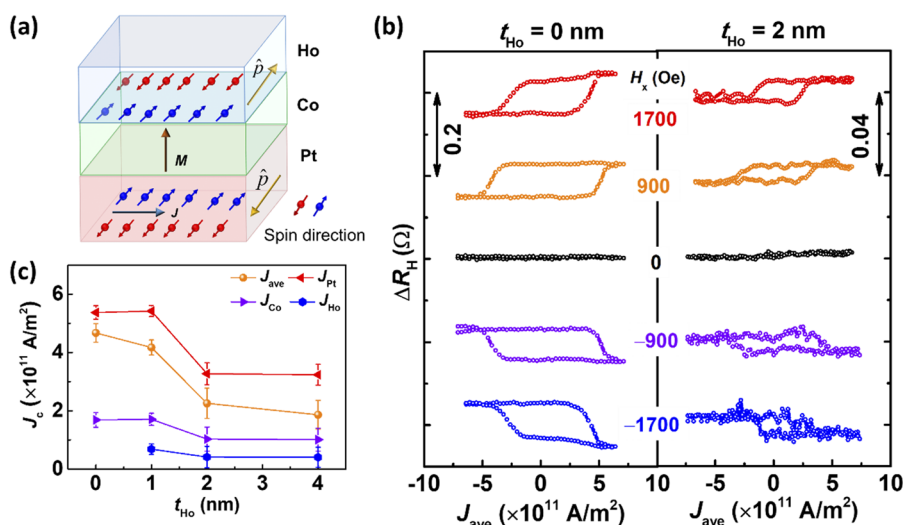


FIG. 2. (a) An illustration of an in-plane charge current J and the induced spin \hat{p} in the investigated Pt/Co/Ho layers. (b) Current-induced magnetic switching curves under the different in-plane bias fields H_x from 1700 to -1700 Oe of Pt/Co/Ho (t_{Ho}) samples for $t_{\text{Ho}} = 0 \text{ nm}$ and $t_{\text{Ho}} = 2 \text{ nm}$. (c) The critical current density J_c as a function of Ho thickness under the in-plane magnetic field $H_x = 900 \text{ Oe}$. J_{ave} indicates the average current density and $J_{\text{Pt,Co,Ho}}$ indicates the current density in each layer.

1700 Oe to -1700 Oe, obtained by sending a series of current pulses with 5 ms duration, for the devices without a Ho layer ($t_{\text{Ho}} = 0$ nm) and with a Ho layer ($t_{\text{Ho}} = 2$ nm). The current is applied along the x -axis, and the maximum amplitude of the pulse current is 22 mA to avoid the high thermal effect in reversing the magnetization. Here, the average current density J_{ave} is calculated from the total current flowing through the whole Pt/Co/Ho system. The change in the Hall resistance ΔR_{H} is detected to monitor the magnetization switching. An IP magnetic field is required to realize the deterministic switching.^{38–40} For $H_x = 0$ Oe, magnetization switching diminishes for both samples. The switching current is reduced with larger H_x .⁴¹ Moreover, the switching loops show opposite polarities by applying H_x in different (i.e., opposite) directions. We summarized that the critical switching current density J_c changes with Ho thickness under $H_x = 900$ Oe, as shown in Fig. 2(c). The critical switching current density J_c was taken from the average current density, which was obtained from dR_{H}/dI curves. Due to the difference in the resistivity of each layer, the current density in each layer of the Pt/Co/Ho system has also been estimated, which is shown in Fig. 2(c). Most of the current flows through the bottom Pt layer (for more details, refer to Sec. S3 of the supplementary material). It can be noticed that J_c reduces when t_{Ho} increases. For the control sample Pt/Co/MgO, the switching average current density J_c is 4.67×10^{11} A m⁻², corresponding to the total power to switch the magnetization of 0.97 W. For $t_{\text{Ho}} = 2$ nm, J_c reduces to 2.26×10^{11} A m⁻². Moreover, the power consumption for magnetization switching drastically reduces to 0.38 W. When t_{Ho} increases to 4 nm, J_c further reduces to 1.86×10^{11} A m⁻², which is roughly two times smaller than that of the control sample Pt/Co/MgO. The steep reduction of 60% in J_c cannot be fully explained by the observed decrease in M_s and K_{eff} , where M_s decreases by 15% and K_{eff} does not change significantly from $t_{\text{Ho}} = 0$ nm to 2 nm. This indicates that the smaller critical switching current density in devices with an interfacial Ho layer is mainly induced by a higher damping-like torque efficiency rather than the change of the magnetic properties.

To better understand the contribution of the SOT-induced magnetization switching arising from the Co/Ho interface, we carried out the harmonic measurements. These measurements enable the quantification of the SOT efficiency and validate the conclusions drawn in the study of current-induced switching. Figures 3(a) and 3(b) show the schematics of harmonic Hall voltage measurements while sweeping an IP external magnetic field in the direction of longitudinal (H_x) and transverse (H_y) to the sending current direction (x -direction). The roles that the DL and FL torques play on the magnetization in the magnetic layer are also shown schematically. Figure 3(c) shows $V_{1\omega}$ and $V_{2\omega}$ obtained from harmonic Hall measurements, as a function of H_x for $t_{\text{Ho}} = 2$ nm with the initial magnetization states to be up (M-up) and down (M-down), respectively. Similarly, Fig. 3(d) shows $V_{1\omega}$ and $V_{2\omega}$ as a function of H_y for $t_{\text{Ho}} = 2$ nm. All the voltages were measured under an average current density J_{ave} of 1.0×10^{11} A m⁻² (much smaller than the critical switching current). The alternative current (I_{ac}) with a frequency of 333 Hz was used in the measurement. It can be noted from Figs. 3(c) and 3(d) that, for the longitudinal H_x and transverse H_y measurements, $V_{1\omega}$ follows the parabolic relation, while $V_{2\omega}$ follows the linear relation. The similar behavior of harmonic voltages is widely reported in PMA systems.^{38,39}

Based on the Hall voltage results, H_{DL} and H_{FL} are extracted using the following equation:³⁷

$$H_{\text{DL(FL)}} = -2 \frac{H_{\text{L(T)}} \pm 2\zeta H_{\text{T(L)}}}{1 - 4\zeta^2}. \quad (1)$$

The longitudinal magnetic field (H_{L}) and transverse field (H_{T}) are defined as $H_{\text{L},\pm} = (dV_{2\omega,x\pm}/dH_x)/(d^2V_{1\omega,x\pm}/dH_x^2)$ and $H_{\text{T},\pm} = (dV_{2\omega,y\pm}/dH_y)/(d^2V_{1\omega,y\pm}/dH_y^2)$, respectively. The \pm sign indicates the magnetization pointing up and down. Moreover, ζ is the ratio of planar Hall resistance (PHE) and anomalous Hall resistance ($R_{\text{PHE}}/R_{\text{AHE}}$). The ratio ζ was measured as 0.16 and 0.078 in the samples without a Ho layer and with 2-nm thick Ho, which has been discussed in Fig. S5 of the supplementary material.^{38,39} Due to the smaller value of ζ , the planar Hall effect in Pt/Co/Ho samples could be neglected. Based on Eq. (1), H_{DL} (H_{FL}) mostly depends on H_{L} (H_{T}) when the external magnetic field is applied along the x -direction (y -direction). In order to avoid an obvious Joule heating, a small current density J_{ave} (the average current density in the range of 5×10^{10} A/m²– 13×10^{10} A/m²) was used in our harmonic measurements. Therefore, the thermal effect could be very weak and, hence, neglected.⁴² Figures 3(e) and 3(f) show H_{DL} and H_{FL} as a function of J_{ave} /the applied electric field E for the sample with $t_{\text{Ho}} = 2$ nm. Both H_{DL} and H_{FL} have a linear dependence on J_{ave}/E , in agreement with the origin of SOT.^{1,37} The magnitude of the current-induced effective fields H_{DL} and H_{FL} increases linearly with the current density J_{ave} (as well as E), implying that the thermal effect is weak. Moreover, the increase of H_{DL} indicates an enhancement of the SOT efficiency. To describe the change of SOT efficiency in this Pt/Co/Ho tri-layer system, the dependence on the electric field E is more appropriate than that with J_{ave} .⁴³ In addition, J_{ave} is less than the current density in the heavy metal Pt layer, resulting in the slightly overestimated result of the SOT efficiency.

Figure 4(a) shows the SOT effective field efficiency per applied electric field χ_{DL}^E (χ_{FL}^E), extracted from the slope $|H_{\text{DL}}/E|$ ($|H_{\text{FL}}/E|$), for samples with different t_{Ho} , where the PHE has been considered to estimate the SOT effective fields accurately. Figure 4(b) shows the SOT effective field efficiency per current density $\chi_{\text{DL}}^{J_{\text{ave}}}$ ($\chi_{\text{FL}}^{J_{\text{ave}}}$). For the control sample with the Pt/Co interface, the H_{DL} efficiency χ_{DL}^E is (0.71 ± 0.13) Oe/(kV/m) due to the contributions from the Pt/Co interface and $\chi_{\text{DL}}^{J_{\text{ave}}}$ is $(2.05 \pm 0.09) \times 10^{-10}$ Oe/(A/m²). For the sample with $t_{\text{Ho}} = 2$ nm, χ_{DL}^E significantly increases to (2.62 ± 0.05) Oe/(kV/m). Moreover, $\chi_{\text{DL}}^{J_{\text{ave}}}$ has been increased to $(9.53 \pm 0.05) \times 10^{-10}$ Oe/(A/m²) significantly. The H_{FL} efficiency χ_{FL}^E is smaller in one order than χ_{DL}^E . When 2-nm Ho was inserted, it also shows an increase to 0.33 from 0.064 Oe/(kV/m).

As previously discussed, the DL SOT efficiency per current density $\xi_{\text{DL}}^{J_{\text{ave}}}$ can be expressed through the relation $\xi_{\text{DL}}^{J_{\text{ave}}} = \frac{2e\mu_0 M_s t H_{\text{DL}}}{\hbar J_{\text{ave}}}$,^{21,29,43} where \hbar is the reduced Planck's constant, e is the charge of an electron, μ_0 is the permeability of vacuum, and t is the thickness of the ferromagnetic layer. In a Pt/Co/Ho system, $\xi_{\text{DL}}^{J_{\text{ave}}}$ relates directly to the effective spin Hall angle $\theta_{\text{SH}}^{\text{eff}}$ of the whole system; thus, $\xi_{\text{DL}}^{J_{\text{ave}}}$ can be considered as an equivalent parameter $\theta_{\text{SH}}^{\text{eff}}$ to describe the SOT efficiency.^{29,43,44} For the control sample, the DL SOT efficiency per current density $\xi_{\text{DL}}^{J_{\text{ave}}}$ is 0.071 ± 0.014 , which is

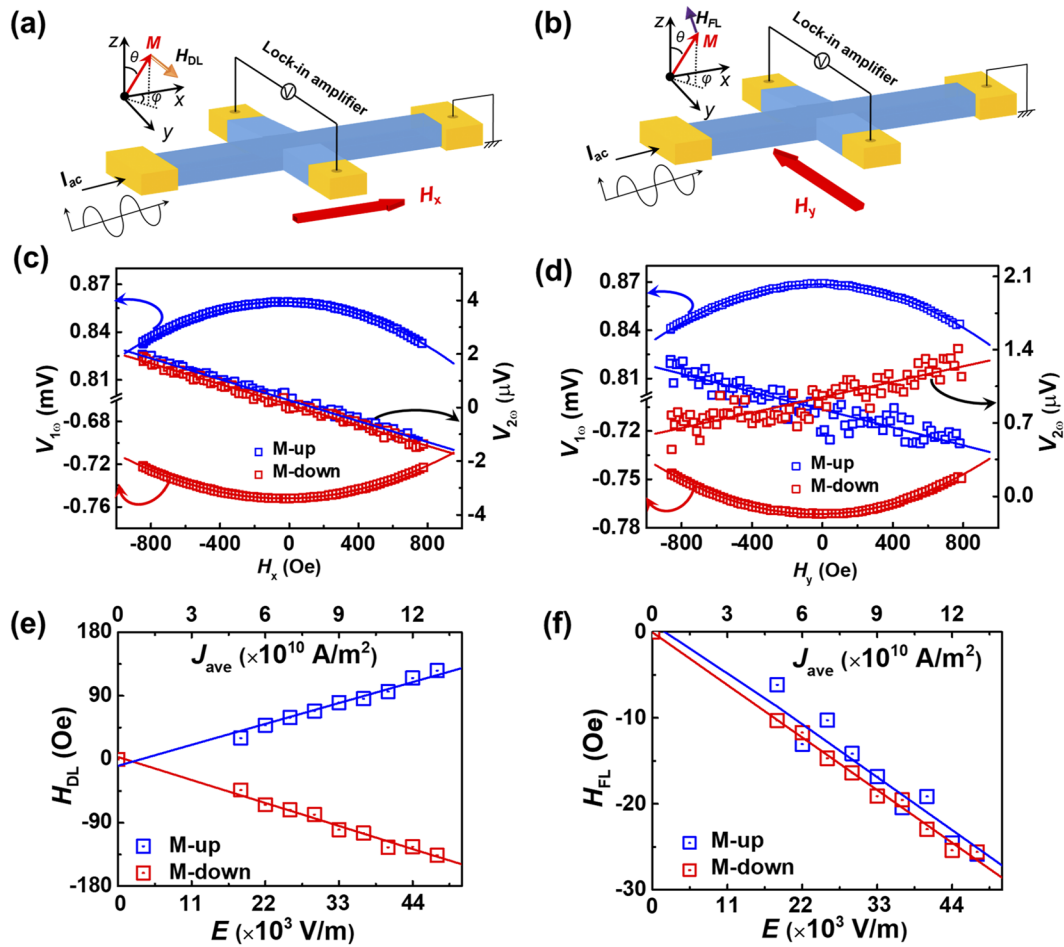


FIG. 3. Illustration of the harmonic measurements set up by sweeping in-plane field in (a) the longitudinal direction H_x and (b) the transverse direction H_y . H_{DL} and H_{FL} refer to the generated effective fields. (c) The first and second harmonic voltage for the sample with $t_{Ho} = 2$ nm with an external in-plane magnetic field H_x applied in the longitudinal direction. (d) The first and second harmonic voltage for the sample with $t_{Ho} = 2$ nm with an external in-plane magnetic field H_y applied in the transverse direction. Calculated (e) H_{DL} and (f) H_{FL} as a function of the average current density J_{ave} /the applied electric field E for the sample with $t_{Ho} = 2$ nm. M-up and M-down refer to the measurements by initially setting the magnetization to be up and down directions, respectively.

similar to the previously reported values in Pt/ferromagnet bilayer systems.^{37,38} It is due to the contributions from the Pt/Co interface. For the sample with $t_{Ho} = 2$ nm, ζ_{DL}^{ave} is increased to 0.256 ± 0.015 , as

depicted in Fig. 5(a). The large DL SOT efficiency per current density ζ_{DL}^{ave} of the Pt/Co/Ho system is attributed to both contributions of Pt and Ho layers. Compared to the Pt/Co/MgO control sample,

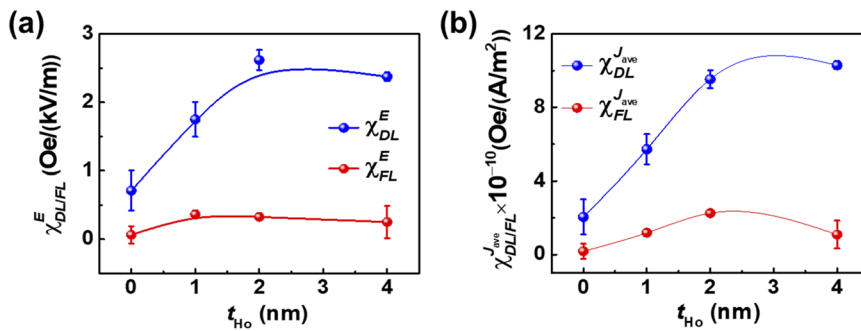


FIG. 4. (a) Calculated SOT field efficiency per applied electric field $\chi_{DL/FL}^E$ and (b) SOT field efficiency per average current density $\chi_{DL/FL}^{J_{ave}}$ as a function of Ho thickness t_{Ho} .

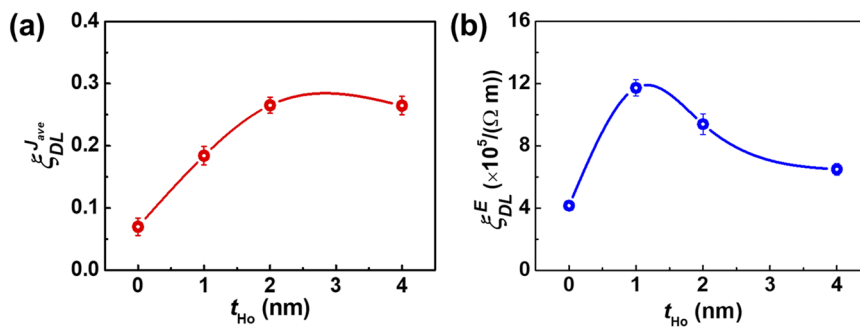


FIG. 5. (a) The damping-like SOT efficiency per current density $\xi_{\text{DL}}^{\text{ave}}$ and (b) the damping-like SOT efficiency per applied electric field $\xi_{\text{DL}}^{\text{E}}$ as a function of Ho thickness t_{Ho} .

the DL SOT efficiency per current density $\xi_{\text{DL}}^{\text{ave}}$ by inserting a Ho layer increases by 0.19.

$\theta_{\text{SH}}^{\text{eff}}$ is not appropriate to describe the spin-torque efficiency in the heterostructures containing more than one spin generator with the discoveries of spin transparency and spin memory loss recently.^{43,45,46} In order to have a better understanding of the SOT efficiency of the Pt/Co/Ho system, the damping-like SOT efficiency per applied electric field $\xi_{\text{DL}}^{\text{E}}$ is also plotted in Fig. 5(b), calculating through the relation $\xi_{\text{DL}}^{\text{E}} = \frac{2e\mu_0 M_s t H_{\text{DL}}}{\hbar E}$.⁴³ For the control sample Pt/Co/MgO, the damping-like SOT efficiency per applied electric field $\xi_{\text{DL}}^{\text{E}}$ is 4.16×10^5 (1/ Ω m). When 1-nm and 2-nm thick Ho layers are inserted on top of the Co layer, the damping-like SOT efficiency $\xi_{\text{DL}}^{\text{E}}$ in the Pt/Co/Ho structure is increased to 11.6×10^5 (1/ Ω m) and 9.4×10^5 (1/ Ω m), respectively.

The high efficiency of SOT in the Pt/Co/Ho structure is attributed to the increase of the spin transparency, and the reduced spin reflection from the Ho layer, which is due to the high conductivity of Ho.^{47,48} Moreover, the negative exchange coupling between Co and Ho layers further enhances the SOT efficiency in the Pt/Co/Ho system.^{29,49,50} The observation of a larger damping-like SOT efficiency while retaining PMA makes this system suitable not only for SOT-MRAM applications but also for the domain wall and skyrmion devices.^{48,51,52} However, the Ho layer capping may introduce potential difficulty in integration based on our current magnetic tunnel junction (MTJ) structure. To compatible with the integration of MTJ by using the tri-layer Pt/ferromagnetic layer (FM1)/Ho structure, a feasible structure has been proposed by depositing an additional ferromagnetic layer (FM2) on top of the capping layer, which is directly coupled with the FM1 layer, forming a Pt/FM1/Ho/FM2/MgO/reference-layer structure.^{52–54} In the proposed structure, the high SOT efficiency can be utilized for writing, which has been demonstrated in the ferrimagnet-based MTJ.^{53–57} The FM2 layer between Ho and MgO is coupled with the reference-layer to form a tunnel magnetoresistive structure, which is mainly meant for the reading process. Moreover, further investigations should also be carried out to improve the thermal stability and optimize the perpendicular magnetic anisotropy for practical applications in perpendicular SOT-MRAM devices.

In conclusion, we report that the insertion of a rare-earth Ho layer on top of a ferromagnetic Co increases the SOT efficiency in Pt/Co/Ho samples. An optimized thickness of inserted Ho is ~ 2 nm, at which the saturation magnetization, anisotropy field, and, in particular, perpendicular magnetic anisotropy are well maintained. The

current-induced magnetization switching and the harmonic measurements show that the critical switching current density is reduced by $\sim 60\%$ and the damping-like SOT field is enhanced by $\sim 200\%$ in the studied Pt/Co/Ho system. Furthermore, the damping-like SOT efficiency per current density of the Pt/Co/Ho system is estimated at around 0.256, which is much larger than the control sample. Our results highlight the significant role of rare-earth metal Ho in the Pt/Co/Ho system to achieve energy-efficient magnetization switching and suggest an alternative path toward the energy-efficient magnetic switching devices.

See the [supplementary material](#) for information about magnetic properties of Pt/Co/Ho thin films with Ho thickness from 1 nm to 10 nm (Fig. S1), transport of ions in matter (TRIM) simulations to understand the interface diffusion effect for samples with different Ho thicknesses (Fig. S2), current distribution in the Pt/Co/Ho system (Fig. S3), thermal effect in Pt/Co/Ho devices with different Ho thicknesses (Fig. S4), planar Hall measurements for Pt/Co/Ho devices (Fig. S5), surface topography (Fig. S6), and dependence of critical switching current density J_c on magnetic parameters (Fig. S7).

AUTHORS' CONTRIBUTIONS

T.J. and W.C. contributed equally to this work.

The work was partially supported by the National Research Foundation of Singapore (Grant Nos. NRF2015-IIP001-001, and NRF2015-IIP003-001 and CRP Grant Nos. NRFCRP9-2011-01 and NRF-CRP21-2018-003). The support from RIE2020 AME IAF-ICP Grant No. I1801E0030 and Programmatic Grant No. A1687b0033 are also acknowledged. This work was supported in part by the National Natural Science Foundation of China (NSFC-12064024) and Natural Science Foundation of Gansu Province (20JR5RA449).

DATA AVAILABILITY

The data that support the findings of this study are available from the corresponding authors upon reasonable request.

REFERENCES

- L. Liu, C.-F. Pai, Y. Li, H. W. Tseng, D. C. Ralph, and R. A. Buhrman, *Science* **336**, 555 (2012).
- S. Bhatti, R. Sbiaa, A. Hirohata, H. Ohno, S. Fukami, and S. N. Piramanayagam, *Mater. Today* **20**, 530 (2017).

- ³K. Cai, M. Yang, H. Ju, S. Wang, Y. Ji, B. Li, K. W. Edmonds, Y. Sheng, B. Zhang, N. Zhang, S. Liu, H. Zheng, and K. Wang, *Nat. Mater.* **16**, 712 (2017).
- ⁴L. Liu, O. J. Lee, T. J. Gudmundsen, D. C. Ralph, and R. A. Buhrman, *Phys. Rev. Lett.* **109**, 096602 (2012).
- ⁵C. O. Avci, K. Garello, I. M. Miron, G. Gaudin, S. Auffret, O. Boulle, and P. Gambardella, *Appl. Phys. Lett.* **100**, 212404 (2012).
- ⁶D. Resnati, A. Goda, G. Nicosia, C. Miccoli, A. S. Spinelli, and C. M. Compagnoni, *IEEE Electron Device Lett.* **38**, 461 (2017).
- ⁷K. Garello, C. O. Avci, I. M. Miron, M. Baumgartner, A. Ghosh, S. Auffret, O. Boulle, G. Gaudin, and P. Gambardella, *Appl. Phys. Lett.* **105**, 212402 (2014).
- ⁸T. Kishi, H. Yoda, T. Kai, T. Nagase, E. Kitagawa, M. Yoshikawa, K. Nishiyama, T. Daibou, M. Nagamine, and M. Amano, in *2008 IEEE International Electron Devices Meeting* (IEEE, 2008).
- ⁹N. Perrissin, S. Lequeux, N. Strelkov, L. Vila, L. Buda-Prejbeanu, S. Auffret, R. C. Sousa, I. L. Prejbeanu, and B. Dieny, in 2018 International Conference on IC Design and Technology (ICICDT), 2018.
- ¹⁰M. Cubukcu, O. Boulle, N. Mikuszeit, C. Hamelin, T. Brächer, N. Lamard, M.-C. Cyrille, L. Buda-Prejbeanu, K. Garello, and I. M. Miron, *IEEE Trans. Magn.* **54**, 81 (2018).
- ¹¹K. Garello, F. Yasin, and G. S. Kar, in *2019 IEEE 11th International Memory Workshop (IMW)* (IEEE, 2019).
- ¹²J. Cao, Y. Chen, T. Jin, W. Gan, Y. Wang, Y. Zheng, H. Lv, S. Cardoso, D. Wei, and W. S. Lew, *Sci. Rep.* **8**, 1355 (2018).
- ¹³Y. Cao, Y. Sheng, K. W. Edmonds, Y. Ji, H. Zheng, and K. Wang, *Adv. Mater.* **32**, 1907929 (2020).
- ¹⁴I. M. Miron, G. Gaudin, S. Auffret, B. Rodmacq, A. Schuhl, S. Pizzini, J. Vogel, and P. Gambardella, *Nat. Mater.* **9**, 230 (2010).
- ¹⁵J. Kim, J. Sinha, M. Hayashi, M. Yamanouchi, S. Fukami, T. Suzuki, S. Mitani, and H. Ohno, *Nat. Mater.* **12**, 240 (2013).
- ¹⁶S. Fukami, T. Anekawa, C. Zhang, and H. Ohno, *Nat. Nanotechnol.* **11**, 621 (2016).
- ¹⁷L. Zhu, K. Sobotkiewich, X. Ma, X. Li, D. C. Ralph, and R. A. Buhrman, *Adv. Funct. Mater.* **29**, 1805822 (2019).
- ¹⁸C.-F. Pai, L. Liu, Y. Li, H. W. Tseng, D. C. Ralph, and R. A. Buhrman, *Appl. Phys. Lett.* **101**, 122404 (2012).
- ¹⁹W. Chen, L. Qian, and G. Xiao, *Sci. Rep.* **8**, 8144 (2018).
- ²⁰T. Suzuki, S. Fukami, N. Ishiwata, M. Yamanouchi, S. Ikeda, N. Kasai, and H. Ohno, *Appl. Phys. Lett.* **98**, 142505 (2011).
- ²¹S. Woo, M. Mann, A. J. Tan, L. Caretta, and G. S. D. Beach, *Appl. Phys. Lett.* **105**, 212404 (2014).
- ²²X. Qiu, Z. Shi, W. Fan, S. Zhou, and H. Yang, *Adv. Mater.* **30**, 1705699 (2018).
- ²³M. Jamali, J. S. Lee, J. S. Jeong, F. Mahfouzi, Y. Lv, Z. Zhao, B. K. Nikolić, K. A. Mkhoyan, N. Samarth, and J.-P. Wang, *Nano Lett.* **15**, 7126 (2015).
- ²⁴J. Han, A. Richardella, S. A. Siddiqui, J. Finley, N. Samarth, and L. Liu, *Phys. Rev. Lett.* **119**, 077702 (2017).
- ²⁵Y. Takeuchi, C. Zhang, A. Okada, H. Sato, S. Fukami, and H. Ohno, *Appl. Phys. Lett.* **112**, 192408 (2018).
- ²⁶W. Chen, G. Xiao, Q. Zhang, and X. Zhang, *Phys. Rev. B* **98**, 134411 (2018).
- ²⁷L. Zhu, D. C. Ralph, and R. A. Buhrman, *Phys. Rev. B* **99**, 180404 (2019).
- ²⁸H. Wang, J. Finley, P. Zhang, J. Han, J. T. Hou, and L. Liu, *Phys. Rev. Appl.* **11**, 044070 (2019).
- ²⁹Q. Y. Wong, C. Murapaka, W. C. Law, W. L. Gan, G. J. Lim, and W. S. Lew, *Phys. Rev. Appl.* **11**, 024057 (2019).
- ³⁰Y. C. Wu, K. K. Meng, J. Miao, X. G. Xu, and Y. Jiang, *J. Magn. Magn. Mater.* **472**, 14 (2019).
- ³¹K. Ueda, C.-F. Pai, A. J. Tan, M. Mann, and G. S. D. Beach, *Appl. Phys. Lett.* **108**, 232405 (2016).
- ³²R. Mishra, J. Yu, X. Qiu, M. Motapothula, T. Venkatesan, and H. Yang, *Phys. Rev. Lett.* **118**, 167201 (2017).
- ³³Y. C. Wu, K. K. Meng, Q. B. Liu, S. Q. Zheng, J. Miao, X. G. Xu, and Y. Jiang, *Phys. Scr.* **95**, 075802 (2020).
- ³⁴W. C. Law, T. L. Jin, X. T. Zhu, R. R. Nistala, N. Thiyagarajah, C. S. Seet, and W. S. Lew, *J. Magn. Magn. Mater.* **477**, 124 (2019).
- ³⁵D.-S. Lee, H.-T. Chang, C.-W. Cheng, and G. Chern, *IEEE Trans. Magn.* **50**, 1 (2014).
- ³⁶T. Yang, T. Matsumoto, H. Yamane, M. Kamiko, and R. Yamamoto, *J. Magn. Magn. Mater.* **198**, 357 (1999).
- ³⁷M. Hayashi, J. Kim, M. Yamanouchi, and H. Ohno, *Phys. Rev. B* **89**, 144425 (2014).
- ³⁸M. Yang, K. Cai, H. Ju, K. W. Edmonds, G. Yang, S. Liu, B. Li, B. Zhang, Y. Sheng, S. Wang, Y. Ji, and K. Wang, *Sci. Rep.* **6**, 20778 (2016).
- ³⁹S. H. Li, G. J. Lim, W. L. Gan, W. C. Law, F. N. Tan, and W. S. Lew, *J. Magn. Magn. Mater.* **473**, 394 (2019).
- ⁴⁰Y. Sheng, K. W. Edmonds, X. Ma, H. Zheng, and K. Wang, *Adv. Electron. Mater.* **4**, 1800224 (2018).
- ⁴¹P. P. J. Haazen, E. Murè, J. H. Franken, R. Lavrijsen, H. J. M. Swagten, and B. Koopmans, *Nat. Mater.* **12**, 299 (2013).
- ⁴²C. O. Avci, K. Garello, M. Gabureac, A. Ghosh, A. Fuhrer, S. F. Alvarado, and P. Gambardella, *Phys. Rev. B* **90**, 224427 (2014).
- ⁴³L. Zhu, D. C. Ralph, and R. A. Buhrman, *Phys. Rev. Lett.* **122**, 077201 (2019).
- ⁴⁴J. Yu, X. Qiu, W. Legrand, and H. Yang, *Appl. Phys. Lett.* **109**, 042403 (2016).
- ⁴⁵C.-F. Pai, Y. Ou, L. H. Vilela-Leão, D. Ralph, and R. Buhrman, *Phys. Rev. B* **92**, 064426 (2015).
- ⁴⁶J.-C. Rojas-Sánchez, N. Reyren, P. Laczkowski, W. Savero, J.-P. Attané, C. Deranlot, M. Jamet, J.-M. George, L. Vila, and H. Jaffrès, *Phys. Rev. Lett.* **112**, 106602 (2014).
- ⁴⁷C. Du, H. Wang, F. Yang, and P. C. Hammel, *Phys. Rev. B* **90**, 140407 (2014).
- ⁴⁸N. Reynolds, P. Jadaun, J. T. Heron, C. L. Jermain, J. Gibbons, R. Collette, R. A. Buhrman, D. G. Schlom, and D. C. Ralph, *Phys. Rev. B* **95**, 064412 (2017).
- ⁴⁹W.-B. Liao, T.-Y. Chen, Y. Ferrante, S. S. P. Parkin, and C.-F. Pai, *Rapid Res. Lett.* **13**, 1900408 (2019).
- ⁵⁰J. Yu, D. Bang, R. Mishra, R. Ramaswamy, J. H. Oh, H.-J. Park, Y. Jeong, P. Van Thach, D.-K. Lee, G. Go, S.-W. Lee, Y. Wang, S. Shi, X. Qiu, H. Awano, K.-J. Lee, and H. Yang, *Nat. Mater.* **18**, 29 (2019).
- ⁵¹L. Liu, X. Zhao, W. Liu, Y. Song, X. Zhao, and Z. Zhang, *Nanoscale* **12**, 12444 (2020).
- ⁵²C. Ma, X. Zhang, J. Xia, M. Ezawa, W. Jiang, T. Ono, S. N. Piramanayagam, A. Morisako, Y. Zhou, and X. Liu, *Nano Lett.* **19**, 353 (2018).
- ⁵³K. Cai, Z. Zhu, J. M. Lee, R. Mishra, L. Ren, S. D. Pollard, P. He, G. Liang, K. L. Teo, and H. Yang, *Nat. Electron.* **3**, 37 (2020).
- ⁵⁴X. Jiang, L. Gao, J. Z. Sun, and S. S. P. Parkin, *Phys. Rev. Lett.* **97**, 217202 (2006).
- ⁵⁵R. A. Duine, K.-J. Lee, S. S. P. Parkin, and M. D. Stiles, *Nat. Phys.* **14**, 217 (2018).
- ⁵⁶A. K. Reza and K. Roy, *J. Appl. Phys.* **126**, 023901 (2019).
- ⁵⁷L. Avilés-Félix, L. Álvaro-Gómez, G. Li, C. S. Davies, A. Olivier, M. Rubio-Roy, S. Auffret, A. Kirilyuk, A. V. Kimel, Th. Rasing, L. D. Buda-Prejbeanu, R. C. Sousa, B. Dieny, and I. L. Prejbeanu, *AIP Adv.* **9**, 125328 (2019).